Electronic Supplementary Material (ESI) for Materials Horizons

Colloidal Oxide Nanoparticle Inks for Micrometer-Resolution Additive Manufacturing of Three-Dimensional Gas Sensors

Hehao Chen, Xinjie Min, Yue Hui, Weiwei Qin, Boyu Zhang, Yuan Yao, Wang Xing, Wei Zhang* and Nanjia Zhou*

Method

Ink preparation

We first dissolved polyethyleneimine (PEI, Sigma-Aldrich, Inc, shanghai, R.P. China) with a certain number-average molecular weight (e.g., M_n = 600, 10000 or 60000 g/mol) in Milli-Q water. A 50 wt% SnO_2 colloidal suspension was created by mixing 20 g SnO_2 nanoparticles (stannic oxide, mean diameter = 50-70 nm, Macklin Inc, Shanghai, P.R. China) and 20 g PEI aqueous solution, and then high-energy ball-milled using a rotation/revolution pulverizer (NP-100, Thinky Co., Ltd., Tokyo, Japan) with 10 g of yttrium-stabilized zirconium oxide beads (Diameter ~ 0.1 mm, Nikkato Co., Ltd., Osaka, Japan), via a 6-time milling cycle, each at 2000 rpm for 1 min and then 400 rpm for 6 mins. The resulting suspension was filtered through a 5-μm syringe filter to eliminate any large agglomerates. Subsequently, PEI-coated SnO_2 nanoparticles were obtained by centrifuging the colloidal suspensions at 9000 rpm for 1 hour to remove excess solvent. After this step, the sediment was redispersed to create a concentrated suspension (~ 35 vol%) by adding an appropriate amount of 30 wt% glycerin aqueous solution (Sigma-Aldrich, Inc, shanghai, R.P. China) as humectant, followed by homogenizing for 5 mins using a Thinky mixer (ARE-300, Thinky Co., Ltd., Tokyo, Japan). The appropriate amount of HNO_3 was added dropwise into the concentrated suspension for promoting its gelation. Finally, the 2 wt% PEO aqueous solution (poly(ethylene oxide) average M_v =1000000 g/mol, Sigma-Aldrich, Inc., Shanghai, China) was added to yield a final PEO concentration of 0.2 wt% and the gel-like inks were once again homogenized.

Ink characterization

The ink rheology was investigated with a controlled stress rheometer (Discovery HR 10, TA Instrument Co., Ltd., US), using a 25 mm-diameter plane plate with 500 μm gap between the parallel plates at 25 °C. A thin layer of low-viscosity silicone oil (viscosity 5 cSt at 25 °C, Sigma-Aldrich, Inc, Shanghai, R.P. China) was employed around the outer edge of the plates to minimize solvent evaporation after as-measured inks were loaded. The rheology measurements were executed in both steady-state flow and oscillatory mode before the inks were pre-sheared at a shear rate of 10 s^{-1} for 1 min to ensure a uniform shear history. In the steady-state flow mode, the ink viscosity was measured as a function of shear rate from 0.1 to 1000 s^{-1}, and fitted by the classical power-law equation:

$$\eta = \mathrm{K}\dot{\gamma}^{n-1} \qquad (S1)$$

Where η is the shear viscosity, K is the flow consistency index and n is the flow behavior index. In the oscillatory mode, the ink storage and loss modulus were measured by stress amplitude sweep at a frequency of 1 Hz.

Zeta potentials (Zeta potential analyzer, Brookhaven Inc., US) and particle size measurements (Wide-angle dynamic light scattering, Brookhaven Inc., US) were carried out on SnO_2 colloidal suspensions (~ 0.0005 wt%) as a function of pH values in the presence and absence of PEI. All measurements were performed with at least 14 cycles at 25 °C and the different pH values of the colloidal suspensions were obtained by HNO_3 or $NH_3 \cdot H_2O$ titration.

The adsorption behavior of PEI on the particles was investigated as follows. The 50 wt% SnO_2 colloidal suspensions were first created as described earlier. These suspensions were titrated by HNO_3 and $NH_3 \cdot H_2O$ for tailoring their pH values, and then mechanically stirred for 24 hours. The SnO_2 nanoparticles were collected by centrifuging 50 wt% SnO_2 colloidal suspensions at 9000 rpm for an hour and redispersed in distilled water with the previous pH values. Thereafter, the suspensions were centrifuged for an hour at 9000 rpm again. Finally, the sediments were dried at 100 °C for 24 h and separated into three aliquots. Weight loss amounts of each aliquot were obtained by TG analysis (TGA/DSC 3+/1600 HT, Mettler-Toledo Co., Ltd,

Switzerland) under air atmosphere from room temperature to 600 °C and averaged as the PEI adsorption amount.

3D printing

Direct ink writing (DIW) was carried out using a dual-drive air-bearing 3-axis microposition platform as shown in figure S9 (Suzhou Zhide Automatic Control Co., Ltd, China), whose motion is commanded by G-code. The SnO_2 nanoparticle inks were loaded on a 3-cc syringe barrel connected attached by luer-lock to glass microcapillaries (Inner diameter (ID) = 3-5 μm produced using a P-2000 micropipette puller, Sutter Instrument Co., Novato, CA, USA). The syringe barrel was installed in a high-pressure dispensing tool (HP3cc, EFD Inc., East Providence, RI, USA), which was connected to a syringe pump (Performus V, EFD Inc., East Providence, RI, USA). The overall dispensing system can produce a maximum dispensing pressure of 700 psi. All 3D printing processes were performed in ambient conditions with a relative humidity of 30- 40 % and a temperature of 22-27 °C. The typical printing parameters for SnO_2 nanoparticle inks were 50 μm/s of printing speed and ~ 30 psi of air pressure. After printing, the SnO_2 structures were annealed at 300 °C for 2 hrs in an air atmosphere for eliminating organic additives. The temperature-dependent morphology and composition evolution of 1D-periodic SnO_2 rods were investigated by using a scanning electron microscope (Gemini450, Carl Zeiss Co., Ltd, Germany) and thermal analysis at heating rates of 10 °C/min in air. The height profiles of SnO_2 rods were generated by a stylus profiler (P-7, KLA-Tencor Co., R. P. China).

Sensor fabrication and gas-sensing test

The printable SnO_2 nanoparticle inks were deposited on the same commercial MEMS-microelectrodes (INS-320, Suzhou Xinmeixin Electronic Technology Co., Ltd, China) with an area of 1×1 mm and a thickness of 0.3 mm. The MEMS-microelectrode adopts a suspended film structure, including a tough SiO_2 film, and the inner layer is covered with S-type platinum as a heating wire to provide a suitable working temperature for the gas-sensing material. All optical images of the printed gas sensor were obtained by microscope (CX40M, Sunny Optical Technology Co., Ltd., P.R. China). The gas-

sensing tests were carried out using homemade gas-sensing equipment modified based on the CGS-1TP intelligent gas sensor analysis system (Beijing Elite Technology Co., Ltd.) with a gas chamber volume of about 18 L. Here, we used programmable multiple output power supplies (GPD-3303S, GWINSTEK) to precisely adjust the current to control the working temperature (test voltage is constantly equal to 5 V). This static gas system was connected to a computer to measure the resistance of the printed sensor, and the relative humidity during the test was about 50 %. The prepared sensors were aged at 300 °C for 48 hours in the air to improve their stability and repeatability before the gas-sensing measurement. During sensing tests, the printed sensors were first placed in a sealed test chamber filled with air, and the test gas (i.e., acetylene) would be introduced after the sensors collected stable signals. The gas concentration in the sealed chamber was adjusted by controlling the ventilation time. When the ventilation was over and the printed sensor response was stable, the upper cover of the test chamber was removed, and the printed sensor began to recover in air.

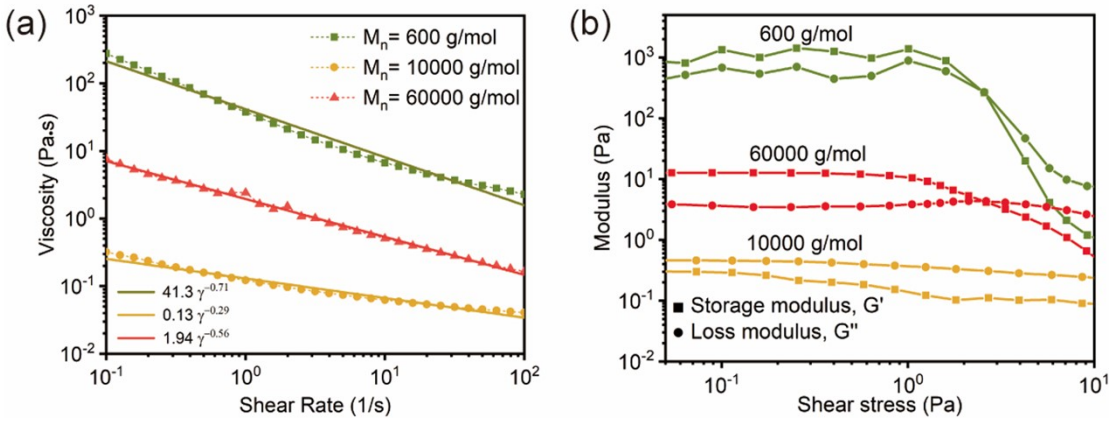

Figure.S1 Rheological characterization of 50 wt% SnO_2 colloidal suspensions containing 8 wt% PEI (by weight of SnO_2 nanoparticles) with varying molar weights of 600, 10000, and 60000 g/mol: (a) viscosities vs. shear rates, (experimental values: dotted lines, fitting values: solid lines) (b) storage and loss modulus vs. shear stresses.

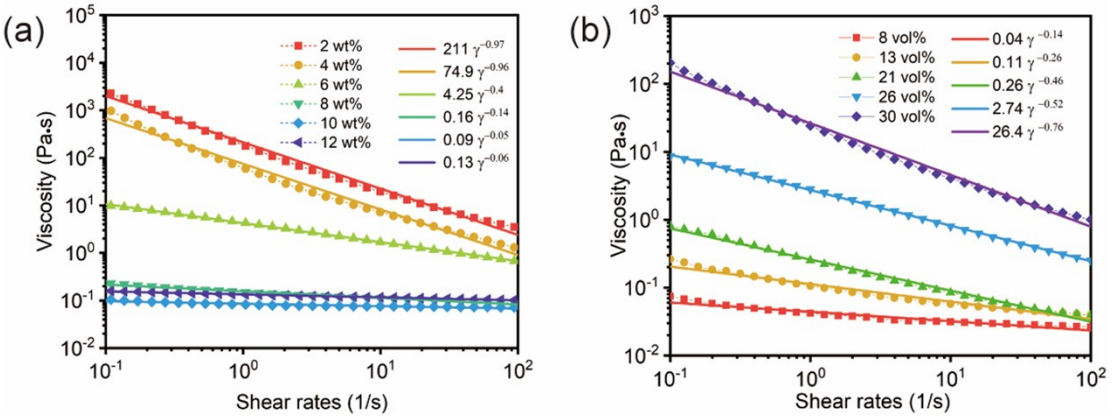

Figure. S2 (a) Dependence of viscosities to shear rates for 50 wt% SnO_2 colloidal suspensions after high energy ball-milling with varying PEI contents ranging from 2 to 12 wt%. (b) Dependence of viscosities to shear rates for high concentrated SnO_2 nanoparticle inks with varying volume fraction from 8 to 30 vol%. (Experimental values: dotted lines, fitting values: solid lines.)

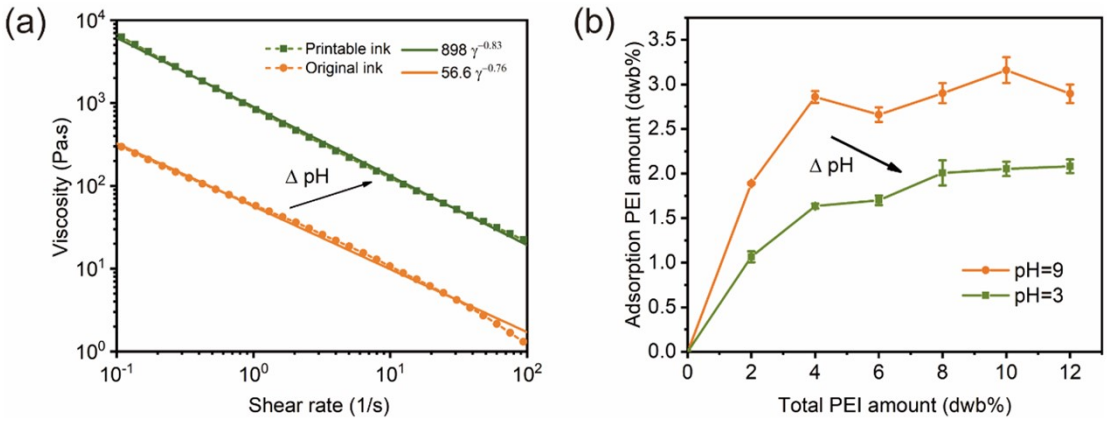

Figure. S3 (a) The change in viscosities of SnO_2 nanoparticle inks after HNO_3 titration (Experimental values: dotted lines, fitting values: solid lines). (b) Adsorption curves for PEI polymer on SnO_2 nanoparticle surface as a function of PEI addition amounts (by dried weight of SnO_2 nanoparticles)

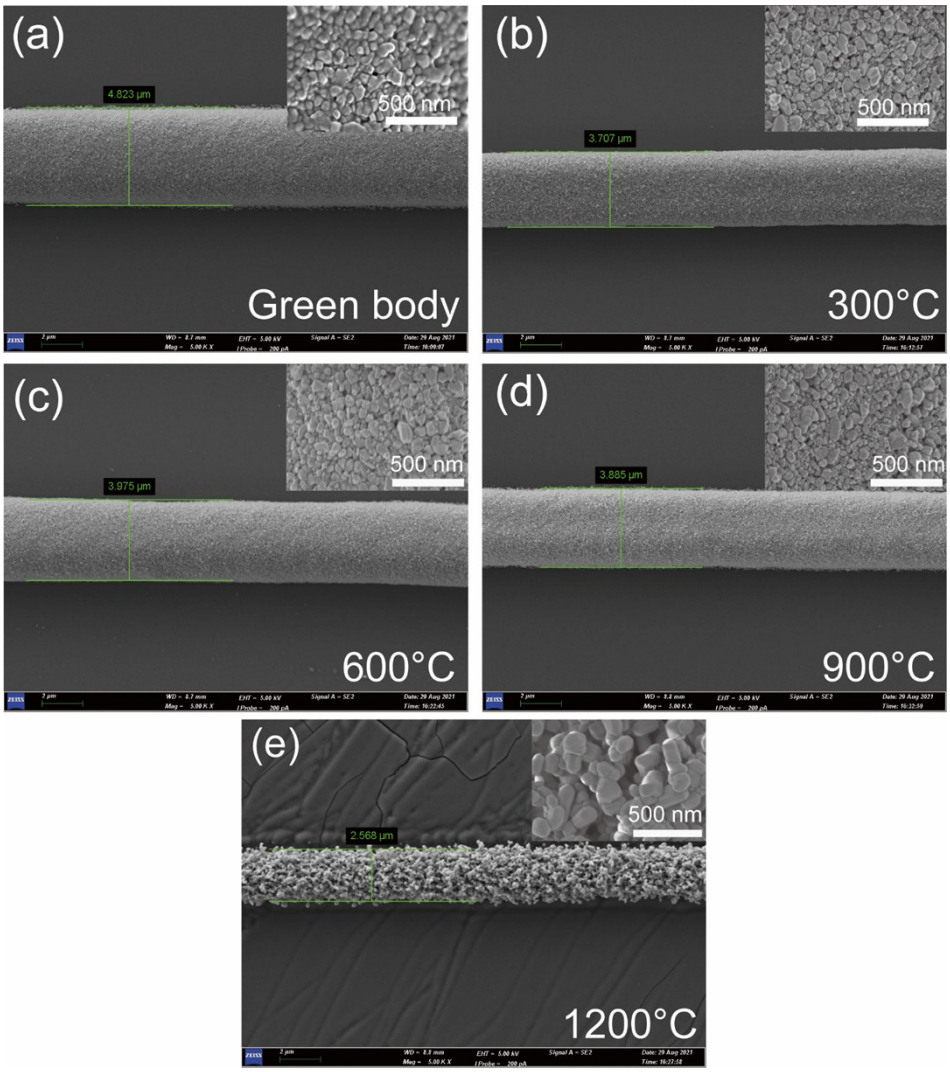

Figure. S4 Surface morphologies of the SnO_2 rods before (a) and after calcination for 2h at 300 °C (b), 600 °C (c), 900 °C (d) and 1200 °C (e) (inset shows the higher magnification images).

Table. S1 Summary of direct ink writing of oxide nanoparticle inks

Materials	**Additives**	**feature size (μm)**	**solid loading (vol%)**	**Methods for regulating rheological properties**	**Ref.**
$YBa_2Cu_3O_x$	Carboxymethyl cellulose sodium; Epoxidized soybean Oil; Water	200	~19	Solid concentration	1
$YBa_2Cu_3O_x$	Dextrin; PEG-400; Solsperse 20000; Water	600	~28.6-~45	Solid concentration	2
TiO_2	Pluronic F-127; Water	200	~14-~26	Solid concentration	3
TiO_2	Dolapix CE64; HPMC; PEI; Water.	150	45.2	Solid concentration	4
Al_2O_3	Synthesized additives; Water	260	~20	Solid concentration	5
Al_2O_3	Wax; Water	200	23-31	Solid concentration	6
Al_2O_3	PAA-PNIPAM; Cellulose; Water	100	40	Thermal stimuli	7
Al_2O_3	Pluronic F-127; Water	150	20.7	Solid concentration	4
ZrO_2	NH_4PAA; Cellulose; Water	210	52	pH value	8
Y_2O_3/ZrO_2	PEGDA; DEG; TPO	65	25-36	Solid concentration	9
ZnO	NH_4PAA; HPMC; Water; PEI	200	44-52	Adding flocculant	10
Al-ZnO	PEGDA; DEG; TPO	65	25-36	Solid concentration	9
Fe_2O_3	PEGDA; DEG; TPO	65	25-36	Solid concentration	9
Fe_3O_4	Synthesized additives; Water	510	~45	Solid concentration	11
VO_2	PDMS	210	~18	Solid concentration	12
SiO_2	Tetraglyme; PDMS;	250	~ 8.6	Solid concentration	13
$BaTiO_3$	PAA; Water	30	45	Ionic concentration	14
$Li_4Ti_5O_{12}$	Water; Ethylene glycol; Glycerol	30	~28	Solid concentration	15
$LiFePO_4$	Water; Ethylene glycol; Glycerol; HPC; HEC	30	~35	Solid concentration	15

$NiFe_2O_4$	PVA; PEG; Solsperse; Water	400	34.5	Solid concentration	16
$BaFe_{12}O_{19}$	PVA; PEG; Solsperse; Water	400	33.9	Solid concentration	16
PZT	NH_4PAA; Water	150	55	pH value	17
SnO_2	PEI; PEO; Glycerol; Water	3-5	~35	pH value	This work

PEGDE: poly(ethylene glycol)diglycidyl ether; ETH: epoThin 2 Hardenner; DEG: diethylene glycol; Dolapix CE64: a commercial dispersant; HPMC: hydroxypropyl methycellulose; PEGDA: poly(ethylene glycol) diacrylate; TPO: diphenyl (2,4,6-trimethylbenzoyl) phosphine oxide; PDMS: polydimethylsiloxane; PEG-400: polyethylene glycol; Solsperse 20000: a commercial dispersant; NH_4PAA: ammonium polyacrylate; PAA-PNIPAM: poly(acrylic acid)-poly(N-isopropylacrylamide); PAA: poly(acrylic acid); HEC: hydroxyethyl cellulose; HPC: hydroxypropyl cellulose; PEI: polyethyleneimine; PEO: poly(ethylene oxide)

Table. S2 Summary of the printed sample types, printing parameters and relative deposited mass.

Sample	Nozzle diameter, D (μm)	Printing path, L (mm)	Mass ratio, M_r^*
D5-S5-L1	5	3.12	3.25
D5-S10-L1	5	1.68	1.75
D5-S20-L1	5	0.96	1
D5-S20-L2	5	1.93	2.01
D5-S20-L4	5	3.85	4.01
D5-S20-L6	5	5.78	6.02
D5-S20-L8	5	7.7	8.02
D20-S20-L1	20	1.6	27.3

*Mass ratio was calculated by the below formula, and reference mass (M_0) is defined as the mass of sparse pattern sample.

$$Mr = \frac{M_x}{M_0} = \frac{V_x}{V_0} = \frac{\left(\pi\frac{D}{2}\right)^2 L}{\left(\pi\frac{D_0}{2}\right)^2 L_0} = \frac{D^2 L}{D_0^2 L_0} \qquad (S2)$$

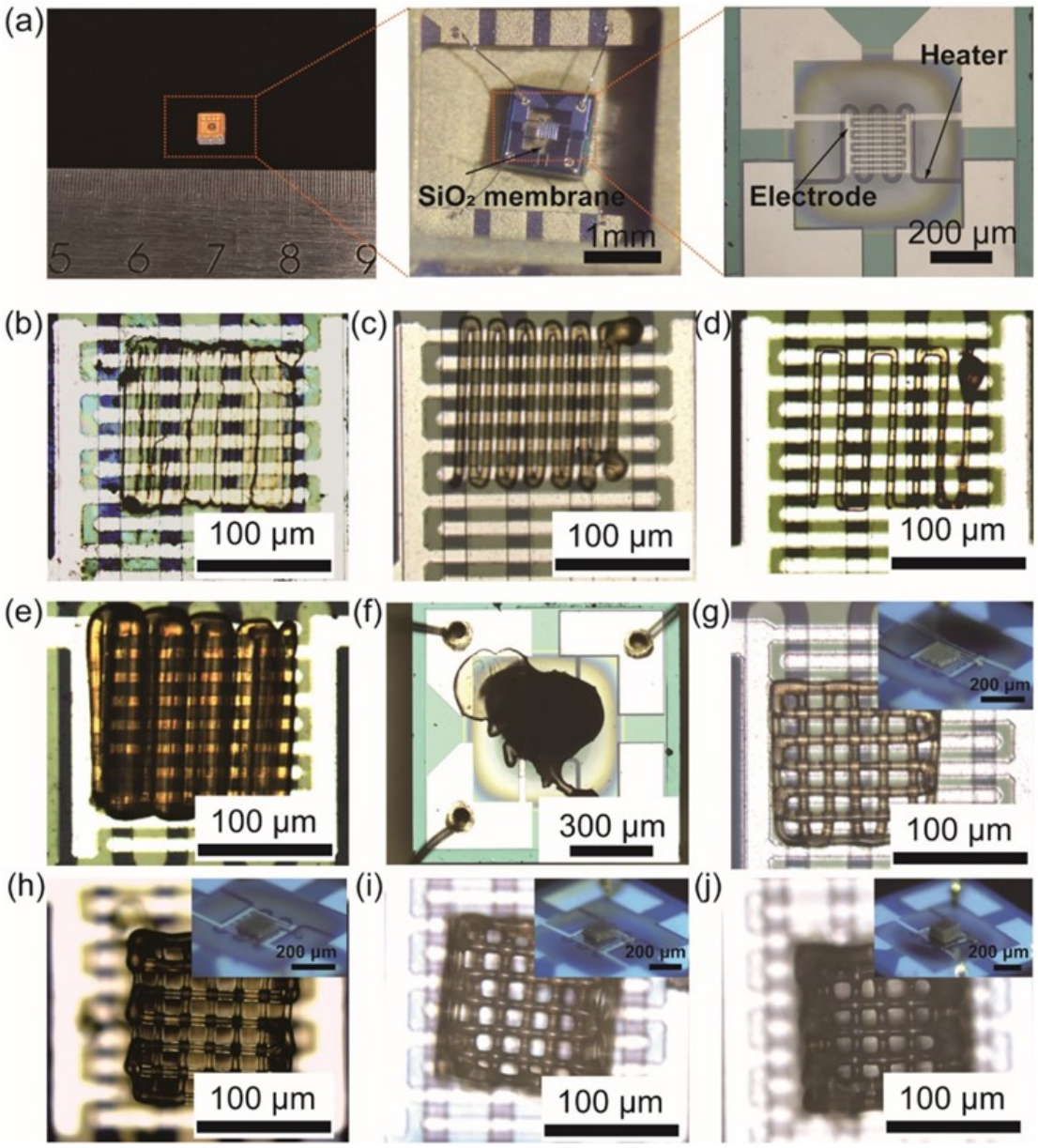

Figure. S5 Optical images of (a) MEMS-based microelectrode and various structured SnO2 gas sensors, i.e., (b) D5-S5-L1, (c) D5-S10-L1, (d) D5-S20-L1, (e) D20-S20-L1, (f) coated sample, (g) D5-S20-L2, (h) D5-S20-L4, (i) D5-S20-L6 and (j) D5-S20-L8.

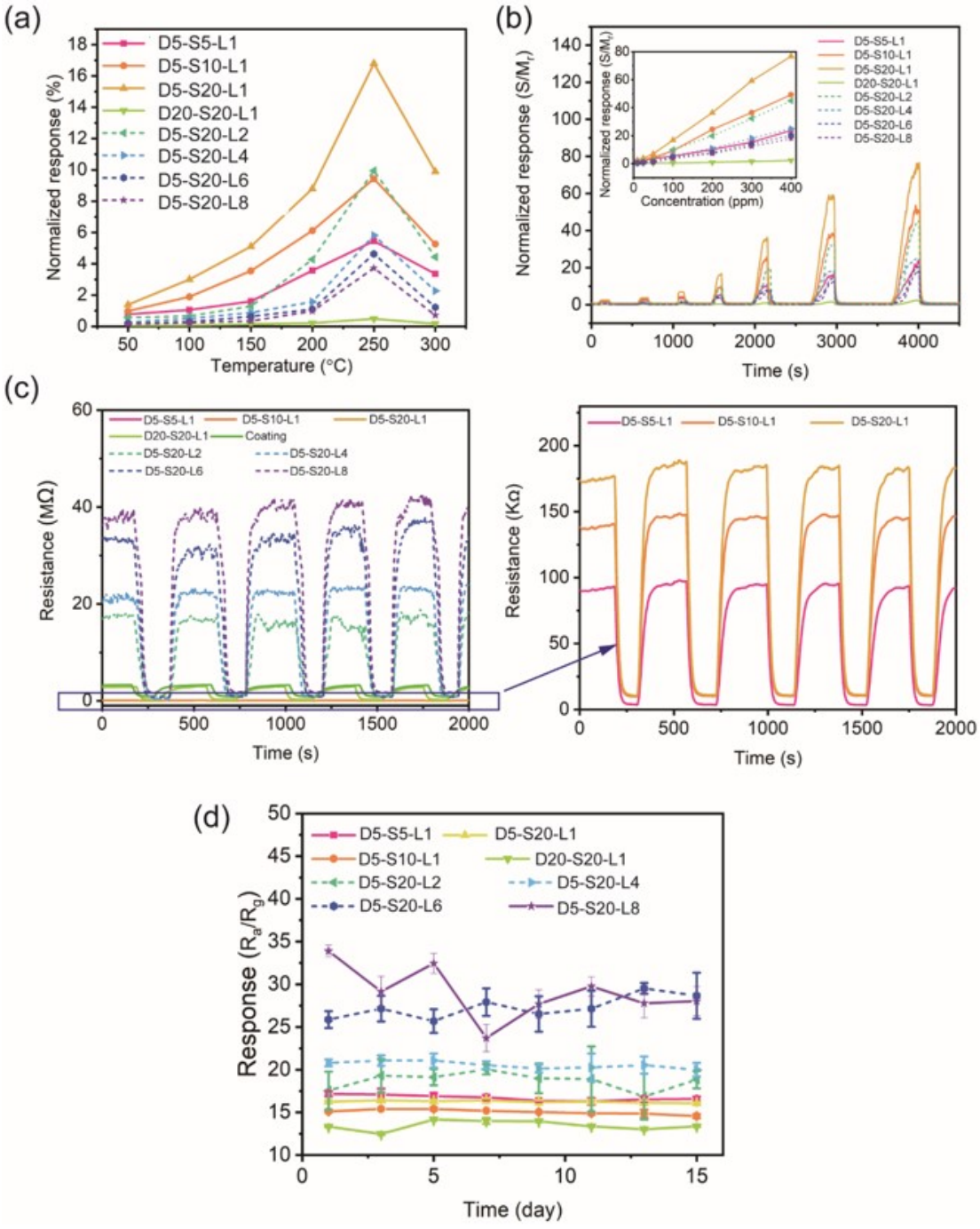

Figure.S6 (a) Normalized gas response to acetylene (100 ppm) for various structured SnO_2 measured at operating temperatures from 50 °C to 300 °C. (b) Gas concentration dependency of the normalized gas response for various structured SnO_2 at an operating temperature of 250 °C. (c) The resistance changes of various structured SnO_2 in response to acetylene (100 ppm) at 250 °C. (d) The long-term stability measurement of printed SnO_2 structures exposed to 100 ppm acetylene at 250 °C.

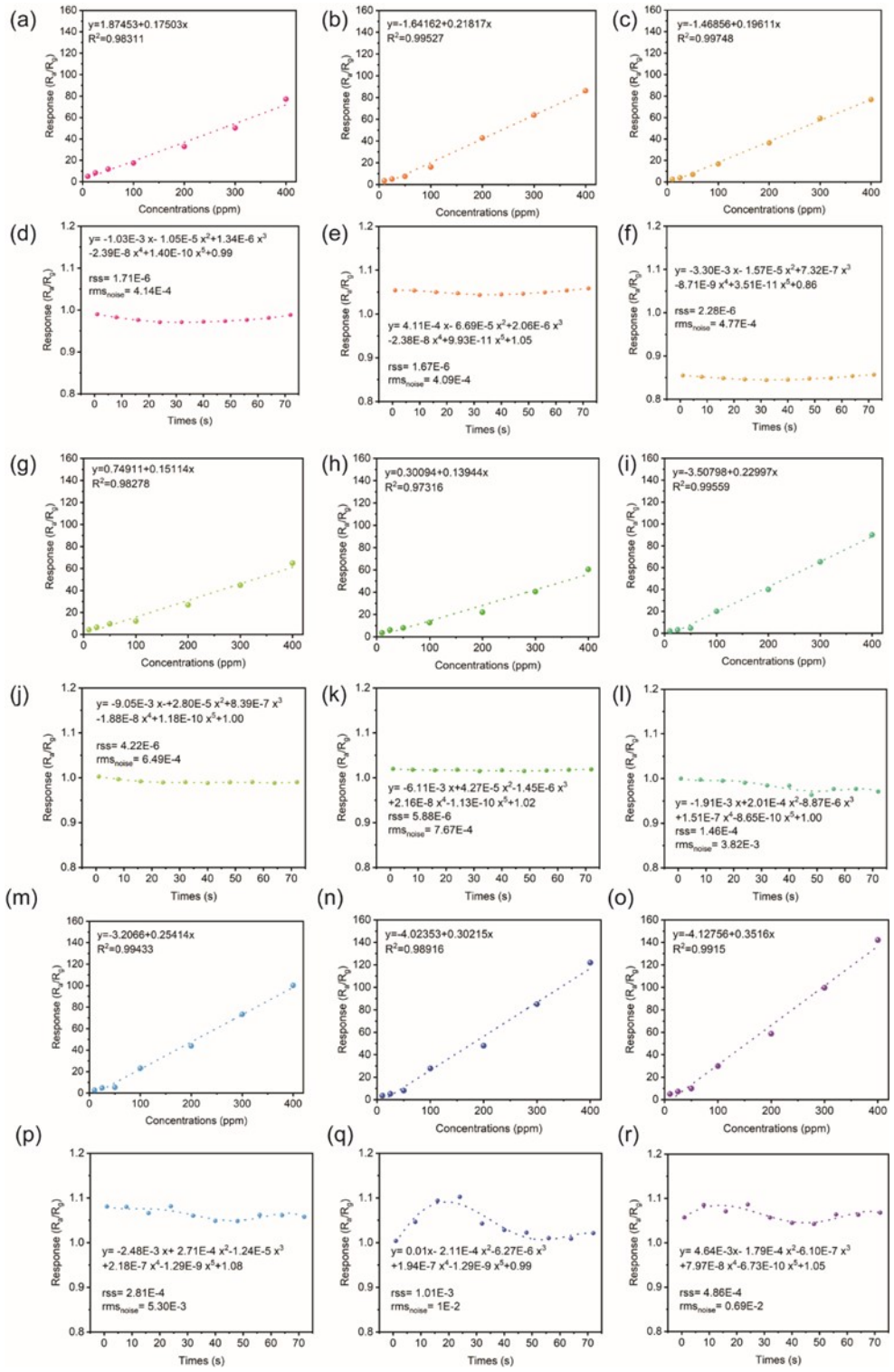

Figure.S7 Linear fit curves of the response to C_2H_2 concentration from all samples: (a) D5-S5-L1, (b) D5-S10-L1, (c) D5-S20-L1, (g) D20-S20-L1, (h) coated sample, (i) D5-S20-L2, (m) D5-S20-L4, (n) D5-S20-L6 and (o) D5-S20-L8. Fifth-order polynomial fit curves of 10 data points taken from at the baselines of printed samples before the C_2H_2 exposure: (d) D5-S5-L1, (e) D5-S10-L1, (f) D5-S20-L1, (j) D20-S20-L1, (k) coated sample, (l) D5-S20-L2, (p) D5-S20-L4, (q) D5-S20-L6 and (r) D5-S20-L8. The above experimental data points are all obtained from figure 5 (d).

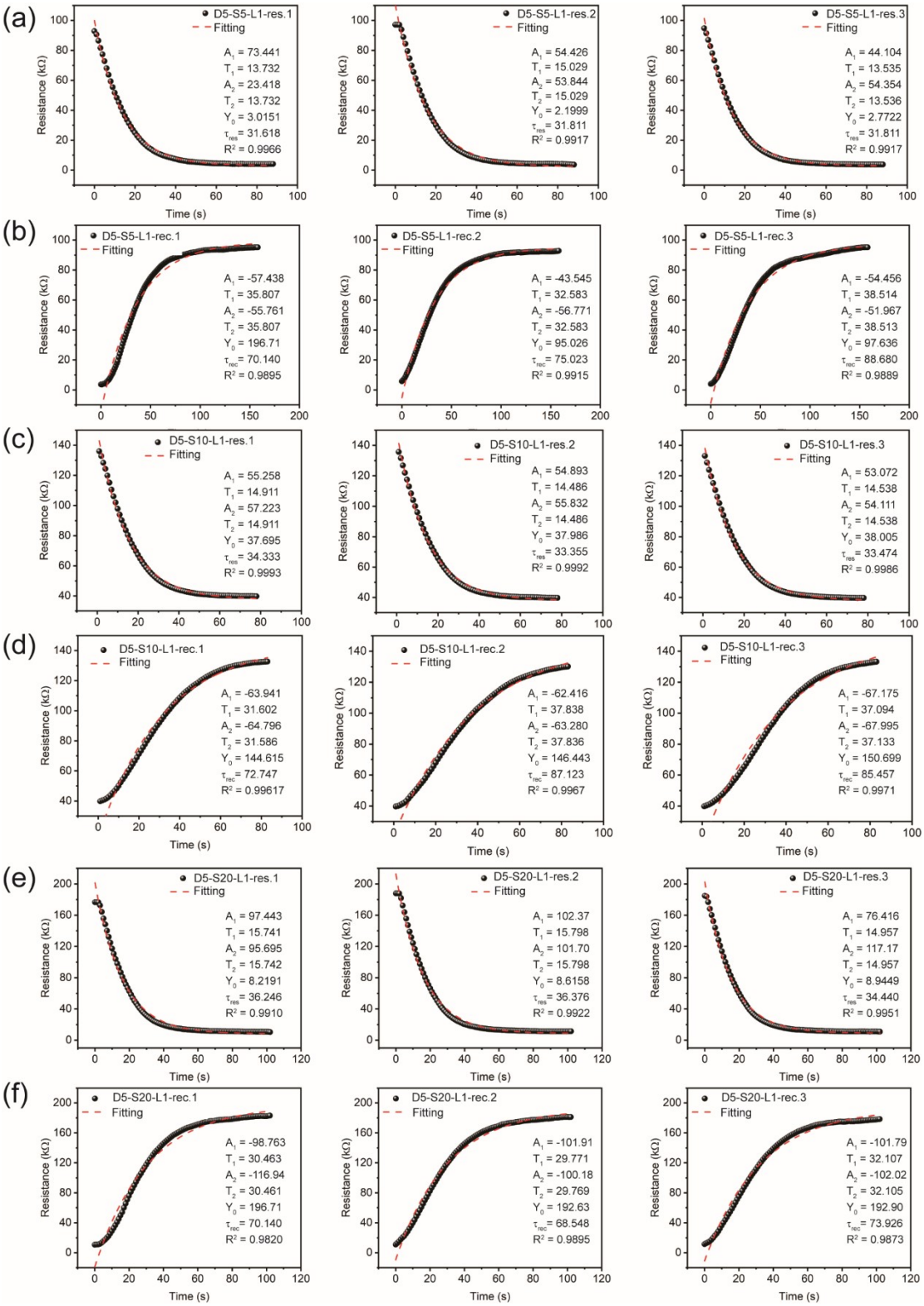

Figure.S8-a Fitting results of three dynamic response/recovery curves for each type of SnO_2 structures, the results are all obtained from figure S6 (c). (To be continued)

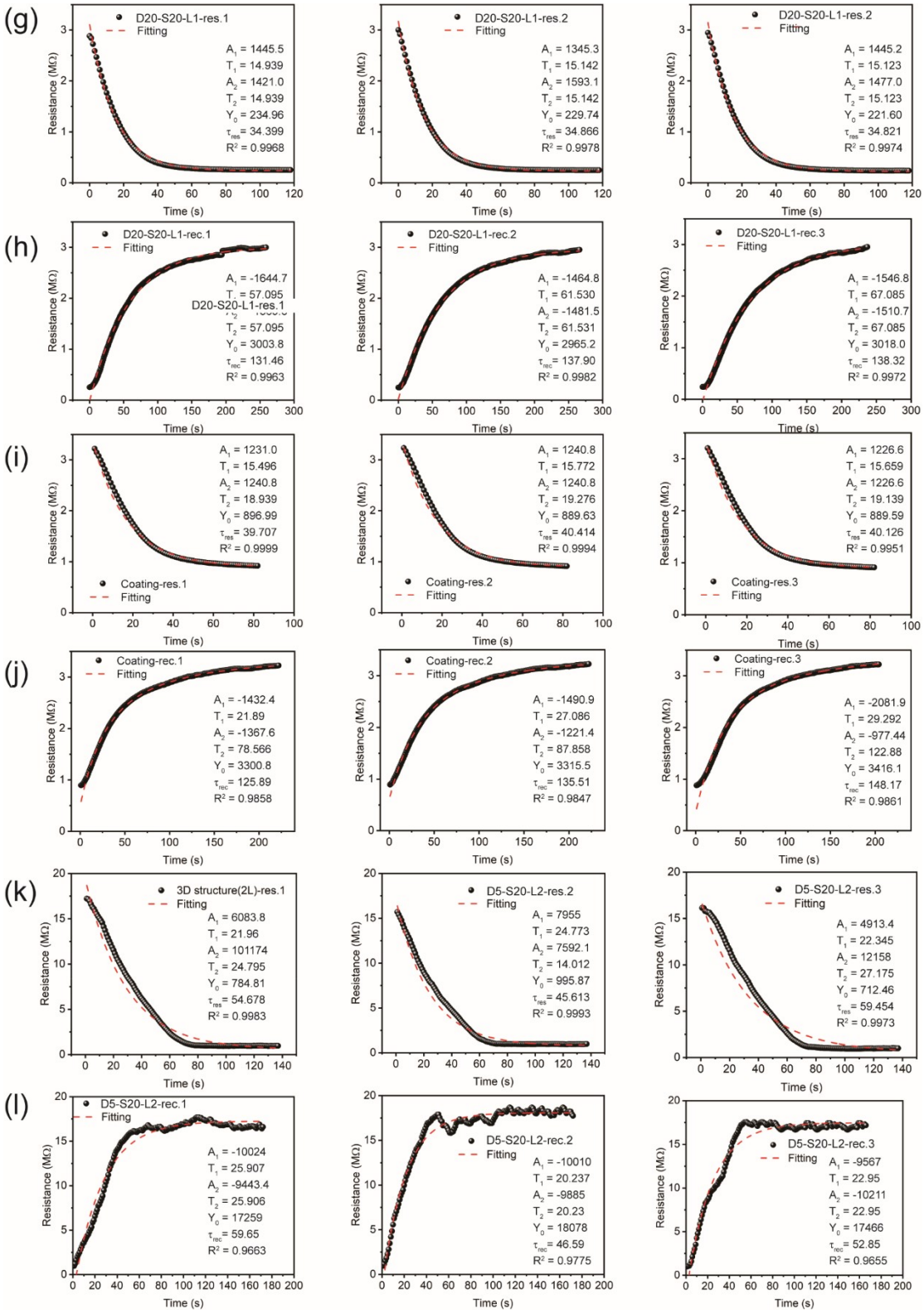

Figure.S8-a Fitting results of three dynamic response/recovery curves for each type of SnO_2 structures, the results are all obtained from figure S6 (c). (To be continued)

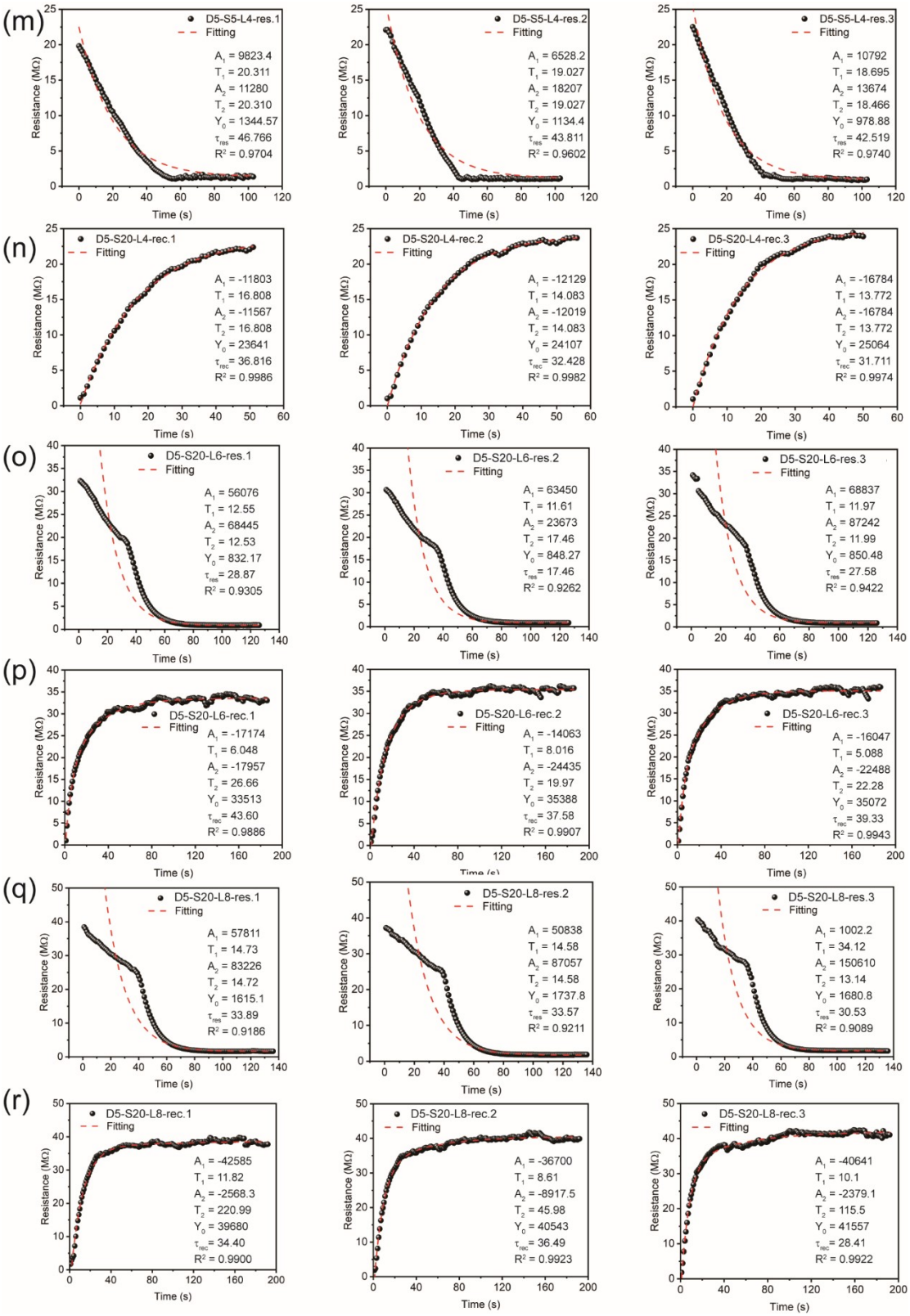

Figure.S8-a Fitting results of three dynamic response/recovery curves for each type of SnO_2 structures, the results are all obtained from figure S6 (c)

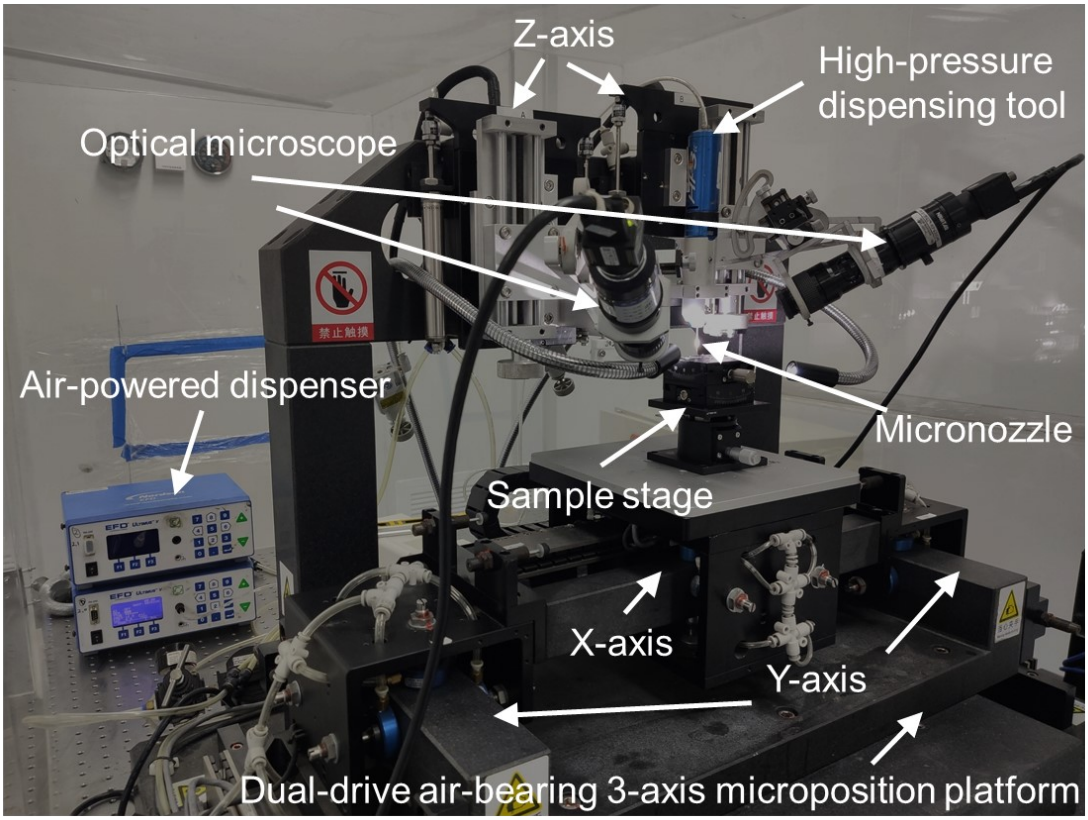

Figure. S9 Photograph of direct ink writing apparatus

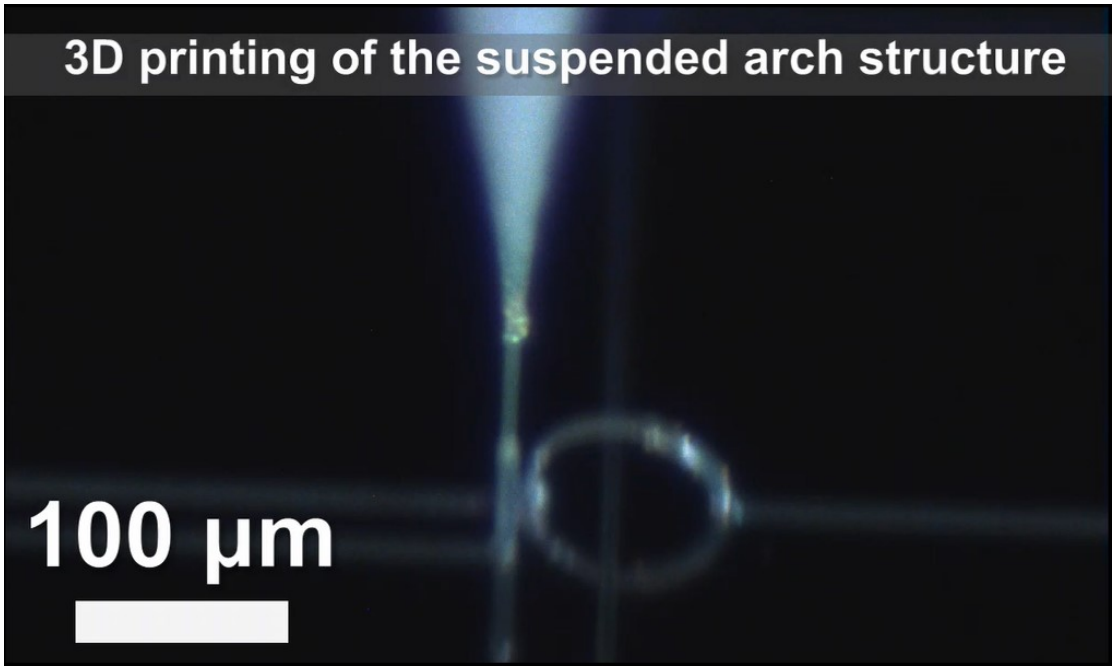

Movie S1. Fabrication of a suspended arch structure by extruding nanoparticle inks through a 5-μm nozzle

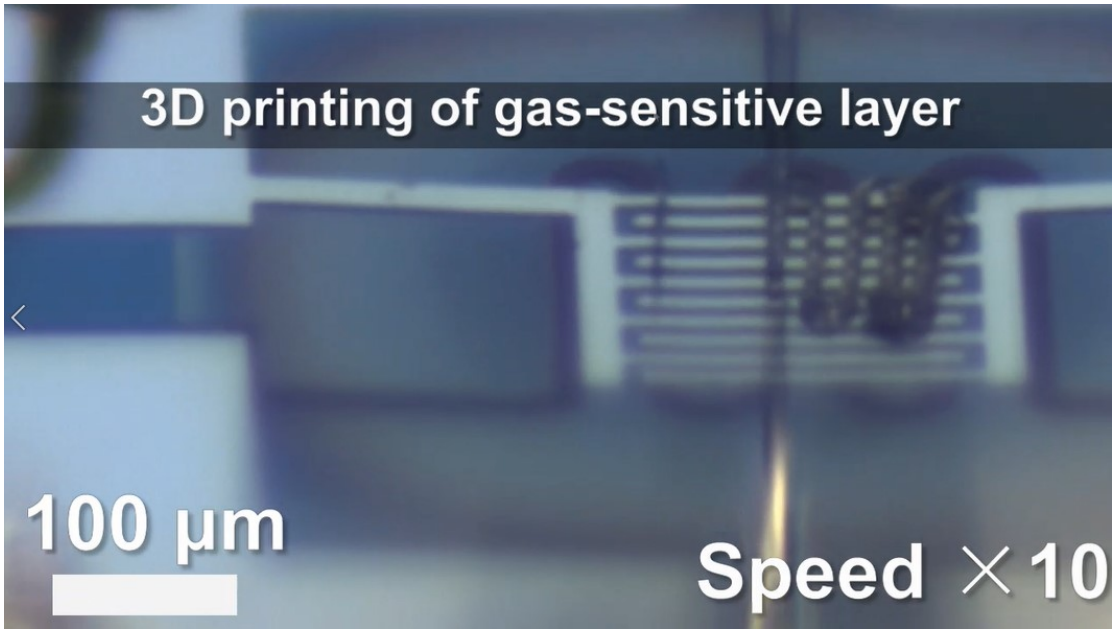

Movie S2. Direct writing of SnO_2 nanoparticle inks through a 5-μm nozzle on the MEMS-microelectrode.

Supplementary Reference

1. B. Zhang, Q. Zhang, P. He, Y. Ma, L. Shen, X. Zhang and Y. Zhou, *Adv. Func. Mater.*, 2021, **31**, e2100680.
2. X. X. Wei, E. Peng, Y. Y. Xie, J. M. Xue, J. Wang and J. Ding, *J. Mater. Chem. C*, 2017, **5**, 3382-3389.
3. W. Guo, Y. Liu, Y. Sun, Y. Wang, W. Qin, B. Zhao, Z. Liang and L. Jiang, *Adv. Funct. Mater.*, 2021, **31**, e2100768.
4. B. Nan, F. J. Galindo-Rosales and J. M. F. Ferreira, *Mater. Today*, 2020, **35**, 16-24.
5. Z. Goharibajestani, O. Akhlaghi, C. Akaoglu, F. Afghah, N. Khani, A. Hodaei, B. Koc and O. Akbulut, *ACS Appl. Polym. Mater.*, 2019, **1**, 3279-3285.
6. J. Maurath and N. Willenbacher, *J. Eur. Ceram. Soc.*, 2017, **37**, 4833-4842.
7. X. Wang, Y. Sun, C. Peng, H. Luo, R. Wang and D. Zhang, *ACS Appl. Mater. Interfaces*, 2015, **7**, 26131-26136.
8. J. Liao, H. Chen, H. Luo, X. Wang, K. Zhou and D. Zhang, *J. Mater. Chem. C*, 2017, **5**, 5867-5871.
9. D. Zhang, E. Peng, R. Borayek and J. Ding, *Adv. Func. Mater.*, 2019, **29**, e1807082.
10. C. R. Tubío, F. Guitián and A. Gil, *J. Eur. Ceram. Soc.*, 2016, **36**, 3409-3415.
11. A. Hodaei, O. Akhlaghi, N. Khani, T. Aytas, D. Sezer, B. Tatli, Y. Z. Menceloglu, B. Koc and O. Akbulut, *ACS Appl. Mater. Interfaces*, 2018, **10**, 9873-9881.
12. R. Wang, W. Yang, S. Gao, X. Ju, P. Zhu, B. Li and Q. Li, *J. Mater. Chem. C*, 2019, **7**, 8185-8191.
13. D. T. Nguyen, C. Meyers, T. D. Yee, N. A. Dudukovic, J. F. Destino, C. Zhu, E. B. Duoss, T. F. Baumann, T. Suratwala, J. E. Smay and R. Dylla-Spears, *Adv. Mater.*, 2017, **29**, e1701181.
14. Q. Li and J. A. Lewis, *Adv. Mater.*, 2003, **15**, 1639-1643.
15. K. Sun, T. S. Wei, B. Y. Ahn, J. Y. Seo, S. J. Dillon and J. A. Lewis, *Adv. Mater*, 2013, **25**, 4539-4543.
16. E. Peng, X. Wei, T. S. Herng, U. Garbe, D. Yu and J. Ding, *RSC Advances*, 2017, **7**, 27128-27138.
17. J. E. Smay, J. C. Iii, B. A. Tuttle and J. A. Lewis, *J. Am. Ceram. Soc.*, 2004, **87**, 293-295.